A Computational and Experimental Examination of the CID of Phosphorylated Serine

George L. Barnes[a,*], Kristopher J. Kolonko[b], Kenneth Lucas[c,1], Klaudia A. Poplawski[c]

[a]*Department of Chemistry*
Illinois State University
Campus Box 4160
Normal, IL 61790-4160
[b]*Stewart's Advanced Instrumentation and Technology (SAInT) Center*
Siena College
515 Loudon Road
Loudonville, NY 12211
[c]*Department of Chemistry and Biochemistry*
Siena College
515 Loudon Road
Loudonville, NY 12211

Abstract

We present and discuss results from direct dynamics simulations, DFT calculations, and experimental measurements of the collision induced dissociation (CID) of *O*-phosphorylation of serine (p-Ser). Moreover, parameters for the interaction potential suitable for use in CID simulations of phosphorylated species were obtained and reported. Within both experiments and simulations, the primary decomposition product is *m/z* 88. This agrees with previous studies, and simulations are consistent with the proposed primary mechanisms suggested in the literature for forming this product. Moreover, the simulations provided insight into subse-

*Corresponding author
Email address: glbarn3@ilstu.edu (George L. Barnes)
[1]Presently at SUNY Upstate Medical University; College of Medicine;766 Irving Avenue; Syracuse, NY 13210

quent decomposition pathways observed experimentally at larger collision energies.

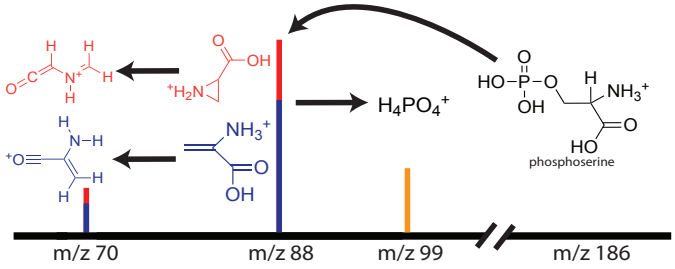

Keywords: Collision Induced Dissociation, Post-Translational Modification, Direct Dynamics Simulation, Graph Theory

1. Introduction

Post-translational modifications (PTMs) are common and expand the functionality of proteins [1–3]. However, they can also complicate protein investigations via tandem mass spectrometry, which is commonly used to study systems of biological interest [4–7]. Phosphorylation is a common post-translational modification (PTM); the impacts of which on collision-induced dissociation (CID) has received considerable attention [8–14]. Phosphorylation is challenging from a tandem mass spectrometry point of view due to the lability of the phosphate group. In addition, the *O*-phosphorylation and *O*-sulfonation result in *m/z* values that require high resolution to distinguish and have similar decomposition pathways.

Direct dynamics simulations [15–21] and *ab initio* calculations have a history of providing significant and impactful insight into the dynamics taking place in tandem mass spectrometry. However, only a few systems that contain PTMs have been studied using these techniques. It can be challenging to undertake direct dynamics simulations since the parameters that define the interaction poten-

tial between the PTM and argon gas are required to simulate explicit argon CID. While the literature already provides the parameters needed to simulate the CID unmodified and sulfonated species, no previous study of a phosphorylated species exists. In this work, we report the necessary interaction parameters to perform direct dynamics simulations of phosphorylated species.

We use these new parameters to study the CID of the *O*-phosphorylation of serine (p-Ser). Both experimental and computational results are reported. Since we have previously examined the CID of the sulfonated analogue, s-Ser [17], comparisons between the two systems will be provided, where appropriate. p-Ser has been the focus of numerous experimental studies, and much work has been performed to elucidate the primary reaction mechanisms. Hence, this is a good test system for these new interaction parameters. Both p-Ser and s-Ser have the same nominal mass of *m/z* 186 and share a prominent CID peak at *m/z* 88 that results from the loss of the PTM as H_3PO_4 and H_2SO_4, respectively. The literature has explored several potential mechanisms for this loss, with the two most prominent being direct loss via β-elimination resulting in protonated 2-amino-propenoic acid and proton transfer from the N-terminus followed by SN2 nucleophilic attack on the β carbon to result in protonated 2-carboxy-aziridine. Both of these pathways will be discussed in greater detail below. It is noteworthy that while p-Ser and s-Ser share the *m/z* 88 peak, they do not have identical CID spectra across a range of collision energies. In particular, s-Ser has a significant population in *m/z* 106 (loss of SO_3) and in *m/z* 140 (loss of H_2O + CO). Both peaks have significantly smaller populations in p-Ser. At larger collision energies, experiments find that p-Ser has secondary decomposition products that have received less experimental focus. The reaction dynamics and structures of these species as revealed by simulations,

are also reported.

An outline for the remainder of the paper is as follows: in Section 2, we provide an overview of our computational and experimental methods; in Section 3, we present our results; and in Section 4, we provide an overview.

2. Methods

We have previously presented the results of both experimental and computational work on s-Ser.[17] We use the same general techniques for the p-Ser system, which are briefly outlined.

2.1. Computational Approach

Within Section 2.1, we will describe the methods used to parameterize CID intermolecular potential energy parameters, the approach to obtaining our starting minimum energy structure, the direct dynamics simulations, the analysis that is performed to obtain a theoretical mass spectrum and outline the types of DFT single point calculations that are performed to characterize the reaction pathways observed in the simulations.

We note that the literature contains numerous examples of the use of direct dynamics simulations to investigate MS2 systems. In addition, recent perspectives on this approach [15, 19, 22] and a tutorial review on the methods involved [19] are available in the literature. We refer the interested reader to those works for more details regarding the approach and provide specific information for our systems of interest below.

2.1.1. Ar - PO_4 Interaction Potential

One method for performing direct dynamics simulations of CID involves modeling the collision between the inert gas argon and the system of interest. The typical approach models the interaction between the argon atom and the system as a sum of Buckingham two-body interactions, i.e.

$$V_{Ar,sys} = \sum_i A_{\mathrm{Ar},i}\, e^{\left(-B_{\mathrm{Ar},i}\, R_{\mathrm{Ar},i}\right)} + \frac{C_{\mathrm{Ar},i}}{R^9_{\mathrm{Ar},i}} \tag{1}$$

where i runs over all atoms within the system of interest and $R_{\mathrm{Ar},i}$ is the distance between the argon and the i^{th} atom of the system. The parameters A, B, and C depend on the chemical identity and environment of the i^{th} atom. This form of interaction is purely repulsive in nature. The literature [23, 24] provides these parameters for several different types of atoms, which were obtained by performing frozen potential energy scans of Ar interacting with small molecules with a similar chemical environment. It is common for these scans to select different orientations that emphasize specific limiting cases for the interactions. All of the *ab initio* electronic energies from each scan are simultaneously fit to obtain the parameters A, B, and C. Obtaining a good fit simultaneously for these limiting orientations provides confidence that the resulting interaction potential will yield good results for all orientations.

The literature does not currently provide parameters for Ar interacting with the phospho- PTM. As this is a common PTM that others may wish to simulate, here we undertake finding these parameters. The literature does provide potential terms for Ar interacting with OH groups, but new terms are needed for Ar interacting with the P atom and oxygen doubly bound to P. Hence, we report potential parameters for the Ar - PO_4^{3-} system suitable for CID calculations. Our frozen potential energy scans at the CCSD(T)/6-31++G** level of theory and basis set

were calculated for two orientations of the Ar – PO_4^{3-} system. The energy at each point was simultaneously fit using a genetic algorithm to a sum of two-body Buckingham potentials. A comparison of the *ab initio* CCSD(T) data and fit is depicted in Figure 1 with the new potential parameters provided in Table 1. We note here that the *ab initio* data has a shallow attractive interaction present. The functional form in Eq. 1 is purely repulsive and designed to reproduce the hard repulsive wall. So while these interaction parameters are suitable for the energy regime of CID simulations, they would not be appropriate for very low energy collisions in which association could occur.

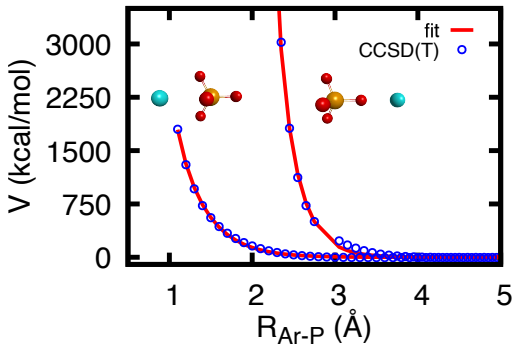

Figure 1: A comparison of the CCSD(T) frozen potential scan and the fit to a sum of two-body Buckingham potentials. The fit simultaneously optimizes both orientations shown above and provides a good reproduction of the repulsive wall.

2.1.2. Direct Dynamics Simulation Method

With all of the "intermolecular" parameters for the Ar – p-Ser collision system on hand, we turn our attention to direct dynamics simulations. The initial structure of p-Ser was determined using Avogadro [25] with the phosphorylation occurring

Table 1: Parameters for the interaction between Ar and P=O with A, B, and C in kcal/mol, $Å^{-1}$, and $Å^9$kcal/mol, respectively.

Parameter Type	*A*	*B*	*C*
Ar – O	56597.86	4.1803	21.200
Ar – P	31361.11	2.8223	450.930

on the side-chain oxygen and the excess proton placed on the N-terminus. Direct dynamics simulations involving protonated peptides are commonly performed with PM6 [17, 26] and the RM1 [16, 21, 22, 26–29] semi-empirical methods. In our study of s-Ser, we found that PM6 outperformed RM1 [17], and expect similar results to be seen here. Hence, the initial structure generated via Avogadro's optimization routines was re-optimized using the PM6 semi-empirical method as implemented in Mopac2016 to yield the initial minimum energy structure [30].

Before starting a direct dynamics simulation, the initial conditions need to be defined. For each trajectory, the internal potential and kinetic energy of the p-Ser system were determined by sampling vibrational and rotational energy from a 300 K distribution via normal modes [31]. p-Ser was then placed 20 Å from the argon atom with a random orientation. The center of mass of p-Ser was then displaced by a randomly selected impact parameter with a maximum value of 3 Å. This maximum impact parameter resulted in a range of translational to internal energy transfers that sufficiently sampled chemical reactivity. The argon and p-Ser were then imparted a relative translational energy consistent with the selected collision energy. One thousand trajectories were calculated for relative collision energies of 3, 5, 7, 9, and 11 eV. As with the maximum impact parameter, these particular col-

lision energies were selected to explore the products produced without producing too many low-mass species resulting from fast fragmentation events [18]. Final analysis was performed either as a function of collision energy or collectively for all collision energies considered depending on the question being answered. Generally speaking, reactivity increased with increasing collision energy.

The direct dynamics simulations themselves were propagated numerically by solving Hamilton's equations of motion using a 6^{th} order symplectic integration scheme [32], for a maximum simulation time of 50 ps with a one fs step size and output written every 50 fs using our in-house simulation package tightly coupled with Mopac2012 [33] to calculate the p-Ser intramolecular potential energy using PM6 [34]. As we are focused on the charged fragments, neutral fragments were removed from the simulation if they were at least 15 Å away from any charged fragments. In addition, a trajectory was halted early if the final charged fragment had an $m/z \leq 60$. Conservation of energy was excellent for all trajectories.

2.1.3. Theoretical Mass Spectra and Reaction Mechanisms

Our in-house simulation software provides the bond order between all QM atoms as a function of time throughout the simulation. A 5 fs window is used to average these bond orders to reduce momentary fluctuations resulting from vibrational motion. The averaged bond order matrix is converted to an adjacency matrix and saved every 50 fs. Post-simulation analysis is performed that identifies the simulation times when fragmentation occurs. Any such events that recombine quickly are removed. Proton motion can be correlated to fragmentation times, allowing for an analysis of the influence of these migrations on dissociation events [35]. It was recently illustrated that this type of information could be combined with a graph theory analysis [16, 36, 37] to define a modified ad-

jacency matrix weighted by the atomic number whose lowest eigenvalue is used to identify unique structures. Graph theory and direct dynamics provide powerful tools for analyzing reaction mechanisms. With the important structures identified using these tools, the energetics are obtained at the ωB97X-D/aug-cc-pVTZ level of theory as implemented in the Gaussian16 software package [38]. We note that many of the mechanisms described here are similar to those seen in s-Ser and were characterized at the same level in our previous work [16].

2.2. Experimental Approach

All chemicals were purchased from Sigma Aldrich and used without further purification. Samples were prepared in mass spectrometry-grade solvents containing a 1:1 mixture of acetonitrile and water. High-resolution mass spectrometry data were acquired on a Bruker Maxis Impact HD (Quadrupole-Time of Flight) spectrometer using sodium formate solution as the mass calibrant and the standard heated electrospray ionization (ESI) source. Pseudo-MS3 experiments were performed utilizing in-source fragmentation. Typical collision energies considered were 5, 10, 12.5, 15, 17.5, 20, 22.5, 25, 30, and 35 eV using nitrogen within the CID cell.

3. Results and Discussion

The experimental measurements of p-Ser are summarized in Figure 2, which presents the normalized intensity for several nominal *m/z* product peaks as a function of collision energy. *m/z* 88 is the only significant product at low to mid collision energies. As the collision energy increases, secondary fragmentation products begin to have larger populations, but *m/z* 88 is still the most significant peak.

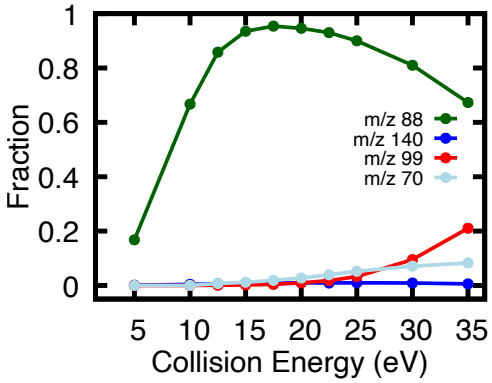

Figure 2: The collision energy dependence of the major peaks observed experimentally. The mother ion, *m/z* 186, is significant at 5 and 10 eV but quickly approaches zero normalized intensity as *m/z* 88 becomes the major species present. At higher collision energies, secondary products also start to be observed.

Examining the simulations and subsequent DFT calculations provides insight into these peaks.

Figure 3 provides a summary and example of the simulated mass spectra. The simulations agree with experiment in that at low collision energies *m/z* 88 is the primary product. However, we do note here that the total reactivity observed within the simulations is significantly less than that in experiment, primarily due to the time scale of the simulations. Moreover, the collision energy range considered is smaller for the simulations to avoid a significant increase in the population of peaks less than *m/z* 50, which our experimental measurements cannot observe.

3.1. m/z 88: Loss of H_3PO_4

The loss of H_3PO_4 to yeild *m/z* 88 is the most common product observed in simulations for most collision energies and corresponds to the loss of the side-chain PTM. This decomposition product was also the most common in our pre-

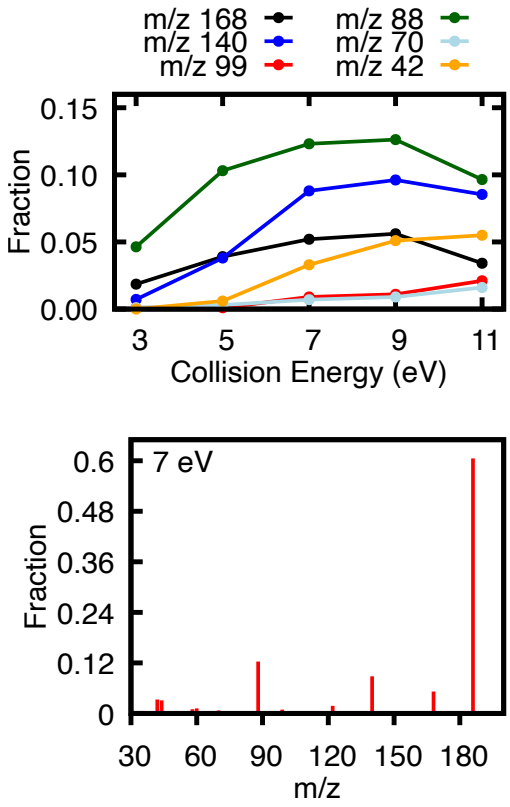

Figure 3: An example simulated mass spectra and the collision energy dependence of notable peaks within simulations. The most commonly observed peak within the simulations is *m/z* 88, which corresponds to the loss of H_3PO_4, i.e., the modified side-chain. As collision energy increases, *m/z* 140 - loss of H_2O + CO - becomes more common.

vious work on s-Ser.[17] The mechanisms described here for p-Ser are direct analogs to those outlined for s-Ser. Formation of *m/z* 88 is also the most dominant peak in experiments at moderate collision energies. This peak has received significant attention within the literature [8–14], with multiple proposed mechanisms suggested based on experimental evidence. This evidence indicates that an SN2 mechanism is likely, which will be described below.

Examining the simulation results shows that there are two major products associated with the *m/z* 88 peak. The most common pathway observed in simulations is a direct loss of H_3PO_4 initiated via a proton transfer from the α-carbon to the oxygen of the phosphoryl group on the side chain. This results in protonated 2-amino propenoic acid (Structure **1**) as the charged product, and is illustrated in the scheme below

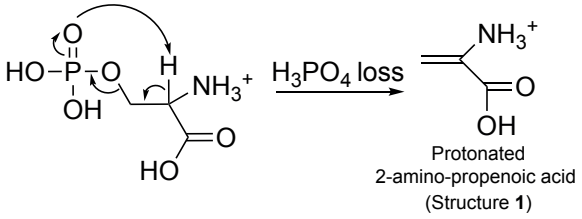

(1)

Our DFT calculations show that this exit channel is $\sim$ 137.2 kJ/mol higher in energy relative to the starting structure, i.e., N-protonated p-Ser. All DFT energies that we report define N-protonated p-Ser as the energy zero. Experimental works in the literature have previously proposed the mechanism in Scheme 1 for both p-Ser and its analogue in s-Ser; however, the most recent experimental works suggest that it is not the primary mechanism.

The second mechanism involves an initial transfer of a proton from the N-terminus to the oxygen of the P=O group on the side chain. Our DFT calculations show that it is energetically more favorable to place the hydrogen on the N-terminus, meaning that unless a conformational change accompanies this transfer, the proton would readily transfer back to the N-terminus. However, if a conformational change does occur, there is a stable minimum energy structure located at $\sim$ 39.9 kJ/mol above the global energy minimum. The simulations show a frequent change in the association between these two protonation sites. However, due to the strong hydrogen bonding present, there is no clearly defined transition between

these protonation states. Once the proton is located on the phosphate group, the N-terminus attacks the first carbon of the side-chain to induce the loss of H_3PO_4 and results in N-protonated 2-carboxy-aziridine (Structure **2**), as illustrated below.

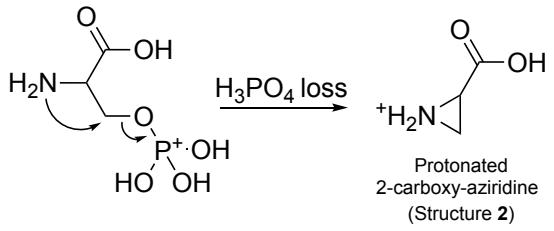

(2)

DFT calculations show that this exit channel is at $\sim$ 181.7 kJ/mol relative to N-protonated p-Ser. Based on experimental evidence reported in the literature, this SN2 mechanism is thought to be the dominant product formed in both p-Ser and s-Ser CID experiments.

Examining our simulations and considering all collision energies, the branching ratio between these two pathways is 0.81 vs. 0.13. Our DFT simulations find that the branched protonated 2-amino propenoic acid (Structure **1**) is lower in energy than the cyclic N-protonated 2-carboxy-aziridine (Structure **2**) by $\sim$ 44 kJ/mol. However, the transition state for Structure **2** is lower by $\sim$ 33 kJ/mol, making N-protonated 2-carboxy-aziridine the more likely product under conditions that favor kinetics rather than thermodynamics. This is consistent with the experimental work of both Lanucara *et al*[9] and Reid *et al*[14]. The simulations predict a qualitatively incorrect branching ratio between these products because the semi-empirical PM6 method, which is employed in the chemical dynamics simulations, treats these two transition states poorly. PM6 reverses the energetic order of these TSs in comparison to the DFT calculations.

Our graph theory analysis shows that these two structures account for a population fraction of 0.94 out of 1 within the peak. N-protonated 2-iminopropanoic

acid accounts for an additional fraction of 0.04. Although this product is not commonly observed within simulations, at the DFT level, it has the lowest energy at $\sim$ 120.4 kJ/mol and could directly convert from Structure **1** via a hydrogen shift. The remaining population fraction - 0.02 - is found in eight uncommonly occurring structures that are unlikely to be stable on the time scale of the experiments and are transient intermediates captured at the end of the simulation time window.

3.2. Subsequent decomposition pathways: m/z 99, 70, 60, and 42

While the majority of focus in the literature has been on the formation of *m/z* 88, some works have noted other experimental peaks [9]. As seen in Figures 2 and 3, our experimental and simulated spectra contain some other peaks. Both *m/z* 99 and 70 are related to structures formed from *m/z* 88. The formation of $H_4PO_4^+$, which corresponds to *m/z* 99, and its relation to *m/z* 88 is described below, while *m/z* 70 results from loss of water from *m/z* 88.

Our simulations indicate that the dominant means of forming $H_4PO_4^+$ is via a continuation of the *m/z* 88 pathways described above, in which the H_3PO_4 group does not immediately "leave" but rather forms a short-lived complex with the *m/z* 88 product. The H_3PO_4 species can then abstract a proton from either the N-terminus or the former side-chains CH_2 group. Forming H_4PO_4 depends on either fast proton abstraction occurring or low translational energy, which allows for the formation of a complex. This species can form from either Structure **1** or **2**. That said, the exit channel starting from Structure **1** is significantly lower in final energy at 156.1 kJ/mol vs. 217.3 kJ/mol for Structure **2**. *m/z* 99 is a minor peak within the simulations that is also seen experimentally. Our experiments show that for most collision energies, it has a low population, but at 35 eV, *m/z* 99 has a relative population fraction of 0.21.

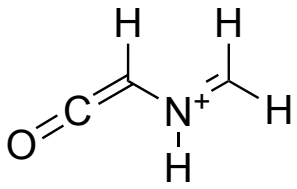

(Structure **3**)

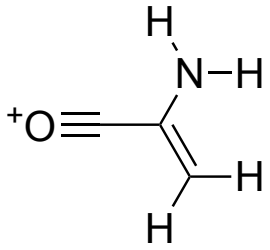

(Structure **4**)

Figure 4: The two *m/z* 70 structures formed from the loss of water from *m/z* 88. Structure **3** is predominately formed from protonated 2-carboxy-aziridine (Structure **2**) and Structure **4** from protonated 2-amino propenoic acid (Structure **1**) via water loss.

m/z 70 is a decomposition product of *m/z* 88 that is seen in experiment and has a population of ~ 0.08 at a collision energy of 35 eV. The simulations predict two stable structures for this peak, Structures 3 and 4 which are shown in Figure 4. The Structure **3** is predominately formed from N-protonated 2-carboxy-aziridine (Structure **2**). This secondary process begins with the abstraction of a proton from the N-terminus by the carbonyl of the C-terminus. This transfer eventually results in ring opening and water loss. These two steps can happen nearly simultaneously or in a step-wise fashion. Structure **4** is predominately formed via water loss from Structure **1** via N- to C-terminus hydrogen transfer. In our simulations, Structure **3** makes up the majority of the peak at low collision energies. At large collision energies, Structure **4** is most common. When considering all collision energies,

Structure **3** is the most commonly observed, with a branching ratio between these two products of 0.86 to 0.1. That said, given the small population of this peak in the simulations, this may not be statistically meaningful. The remaining population within the peak is identified as intermediates that would result in one of the two structures in Figure 4 given enough simulation time. In simulations, *m/z* 42 is formed through two different pathways, one of which is the further water loss from *m/z* 70, and is the primary pathway observed. *m/z* 42 can also be formed by loss of H_3PO_4 from *m/z* 140, which is discussed below.

Our previous simulations on unmodified serine found that the primary decomposition product was *m/z* 60. This peak is also present in the theoretical p-Ser mass spectrum and increases with increased collision energy. While there is some diversity in how this peak forms, it is seen that one of the primary means is through an initial loss of HPO_3 to regenerate N-protonated serine. This intermediate subsequently losses water and CO to form N-protonated 2-Iminoethanol.

3.3. m/z 168 and 140

The peaks at *m/z* 168 and 140 represent a distinct reaction pathway from that of *m/z* 88 and correspond to the loss of water, and loss of water and CO, respectively. Neither represents major peaks in experiment, but *m/z* 140 is observed with a normalized intensity of at most $\sim$ 1%. Although one might expect to find that *m/z* 168 is an intermediate for *m/z* 140, and that can occur; in fact, the simulated *m/z* 168 peak most commonly arises from the loss of water from the phosphate group due to N-terminus attack on the P to form a five-membered ring structure. In contrast, *m/z* 140 most commonly occurs via the loss of the C-terminus. While *m/z* 140 is seen in our experimental measurements, *m/z* 168 is not.

Since the simulations overestimate both of these peaks compared to the exper-

iment, we wished to ensure that this was not indicative of a deficiency in the new CID interaction parameters we reported here. Hence, additional simulations were performed using internal energy excitation rather than a direct collision event with argon. The internal energy was set to 606.7 kJ/mol, which is the average energy transferred to internal degrees of freedom following a collision with argon at 7 eV. Both *m/z* 140 and 168 are seen in these simulations with a significant population. This suggests that the interaction parameters are not at fault, but rather the semi-empirical method itself results in an overestimate of these pathways. This deficiency is more noticeable in p-Ser than in s-Ser given that the *m/z* 140 path has significant population as reported in the experimental work of by Polfer and co-workers [39]. Hence, it was not out of place to see this peak in the s-Ser simulations [17]. This observation suggests that the loss of the PTM is preferred significantly over the loss of the C-terminus in p-Ser and results in a dramatic reduction the experimentally observed population of *m/z* 140 compared to s-Ser.

4. Summary

This work represents the first simulations of the phosphorylation post-translational modification, and we have reported potential energy interaction parameters suitable for future argon CID simulations that are based on high-level CCSD(T)/6-31++G** *ab initio* calculations. These interactions were fit to two-body Buckingham parameters using a genetic algorithm and focus on reproducing the repulsive wall of the interaction.

Our simulations recover the major experimental decomposition product, namely loss of H_3PO_4. The mechanisms observed in simulations are consistent with those previously proposed. It is accepted that the SN2 mechanism is likely the dominant

pathway in experiment, while our simulations show the β elimination pathway as the primary mechanism. This is likely due to the energetics of the semi-empirical method used.

Subsequent decomposition products are seen in both simulations and experiments. *m/z* 99 results from the formation of H_4PO_4, which is seen in simulations to occur due to a complex forming between the products of the primary pathway. *m/z* 70 is seen experimentally and can be attributed to water loss from the primary *m/z* 88 peak. Two stable structures are seen in simulations for this peak, one for each of the most common structures within the *m/z* 88 peak. *m/z* 42, which has also been observed in previous experimental work, was seen in our simulations and results from loss of water from *m/z* 70.

In contrast to s-Ser, *m/z* 140 - lose of H_2O + CO - is not a common product observed in experimental work. However, this peak is observed in the present simulations and our previous work on s-Ser. The presence of *m/z* 140 is likely not a deficiency of the new CID interaction parameters but likely due to the semi-empirical method used for the direct dynamics simulations. It is interesting that s-Ser and p-Ser display a qualitative difference between their CID spectra. This is perhaps due to differences between the sulfur and phosphate binding energy.

5. ACKNOWLEDGEMENTS

The authors acknowledge the generous support from the National Science Foundation under Grant No. 2301606. GLB is a member of the MERCURY consortium, which receives support through National Science Foundation grant No. CHE-2018427.

References

[1] A. Kumar, V. Narayanan, A. Sekhar, Characterizing post-translational modifications and their effects on protein conformation using nmr spectroscopy, Biochemistry 59 (2020) 57–73. doi:10.1021/acs.biochem.9b00827.

[2] H. Ryšlavá, V. Doubnerová, D. Kavan, O. Vaněk, , Journal of Proteomics 92 (2013) 80–109. doi:10.1016/j.jprot.2013.03.025.

[3] C. Boscher, J. W. Dennis, I. R. Nabi, , Current Opinion in Cell Biology 23 (2011) 383–392. doi:10.1016/j.ceb.2011.05.001.

[4] R. G. Cooks, T. Ast, T. Pradeep, V. H. Wysocki, Reactions of ions with organic surfaces, Accounts of Chemical Research 27 (1994) 316–323. doi:10.1021/ar00047a001.

[5] I. A. Papayannopoulos, The interpretation of collision-induced dissociation tandem mass spectra of peptides, Mass Spectrometry Reviews 14 (1995) 49–73. doi:10.1002/mas.1280140104.

[6] E. R. Williams, Tandem ftms of large biomolecules., Analytical chemistry 70 (1998) 179A–85A. doi:10.1021/ac981773x.

[7] V. H. Wysocki, K. E. Joyce, C. M. Jones, R. L. Beardsley, Surface-induced dissociation of small molecules, peptides, and non-covalent protein complexes., Journal of the American Society for Mass Spectrometry 19 (2008) 190–208. doi:10.1016/j.jasms.2007.11.005.

[8] C. M. Potel, S. Lemeer, A. J. Heck, Phosphopeptide fragmentation and site

localization by mass spectrometry: An update, Analytical Chemistry 91 (2019) 126–141. doi:10.1021/acs.analchem.8b04746

[9] F. Lanucara, B. Chiavarino, D. Scuderi, P. Maitre, S. Fornarini, M. E. Crestoni, Kinetic control in the cid-induced elimination of h3po4 from phosphorylated serine probed using irmpd spectroscopy, Chem. Commun. 50 (2014) 3845–3848. doi:10.1039/C4CC00877D.

[10] J. Laskin, R. P. Kong, T. Song, I. K. Chu, Effect of the basic residue on the energetics and dynamics of dissociation of phosphopeptides, International Journal of Mass Spectrometry 330-332 (2012) 295–301. doi:10.1016/j.ijms.2012.09.013.

[11] M. Rožman, Modelling of the gas-phase phosphate group loss and rearrangement in phosphorylated peptides, Journal of Mass Spectrometry 46 (2011) 949–955. doi:10.1002/JMS.1974.

[12] P. J. Boersema, S. Mohammed, A. J. Heck, Phosphopeptide fragmentation and analysis by mass spectrometry, Journal of Mass Spectrometry 44 (2009) 861–878. doi:10.1002/JMS.1599.

[13] A. M. Palumbo, J. J. Tepe, G. E. Reid, Mechanistic insights into the multistage gas-phase fragmentation behavior of phosphoserine- and phosphothreonine-containing peptides, Journal of Proteome Research 7 (2008) 771–779. 10.1021/PR0705136

[14] G. E. Reid, R. J. Simpson, R. A. O'Hair, Leaving group and gas phase neighboring group effects in the side chain losses from protonated serine

and its derivatives, Journal of the American Society for Mass Spectrometry 11 (2000) 1047–1060. doi:10.1016/S1044-0305(00)00189-6.

[15] A. M. Somer, V. Macaluso, G. L. Barnes, L. Yang, S. Pratihar, K. Song, W. L. Hase, R. Spezia, Role of chemical dynamics simulations in mass spectrometry studies of collision-induced dissociation and collisions of biological ions with organic surfaces, Journal of the American Society for Mass Spectrometry 31 (2020) 2–24. doi:10.1021/jasms.9b00062.

[16] K. Lucas, A. Chen, M. Schubmehl, K. J. Kolonko, G. L. Barnes, Exploring the effects of methylation on the cid of protonated lysine: A combined experimental and computational approach, Journal of the American Society for Mass Spectrometry 32 (2021) 2675–2684. doi:10.1021/jasms.1c00225.

[17] K. Lucas, G. L. Barnes, Modeling the effects of o-sulfonation on the cid of serine, Journal of the American Society for Mass Spectrometry 31 (2020) 1114–1122. doi:10.1021/jasms.0c00037.

[18] G. L. Barnes, A. Shlaferman, M. Strain, Fast fragmentation during surface-induced dissociation: An examination of peptide size and structure, Chemical Physics Letters 754 (2020) 137716. doi:10.1016/j.cplett.2020.137716.

[19] S. Pratihar, G. L. Barnes, W. L. Hase, S. Pratihara, G. L. Barnes, W. L. Hase, Chemical dynamics simulations of energy transfer, surface-induced dissociation, soft-landing, and reactive- landing in collisions of protonated peptide ions with organic surfaces, Chemical Society reviews 45 (2016) 3595–3608. doi:10.1039/C5CS00482A.

[20] S. Pratihar, G. L. Barnes, J. Laskin, W. L. Hase, Dynamics of protonated peptide ion collisions with organic surfaces. consonance of simulation and experiment., The journal of physical chemistry letters 7 (2016) 3142–3150. doi:10.1021/acs.jpclett.6b00978.

[21] D. Frederickson, M. McDonough, G. L. Barnes, A computational comparison of soft landing of alpha-helical vs globular peptides, Journal of Physical Chemistry B 122 (2018) 9549–9554. doi:10.1021/acs.jpcb.8b06232.

[22] G. L. Barnes, W. L. Hase, Energy transfer, unfolding, and fragmentation dynamics in collisions of n-protonated octaglycine with an h-sam surface., Journal of the American Chemical Society 131 (2009) 17185–17193. doi:10.1021/ja904925p.

[23] O. Meroueh, W. L. Hase, Collisional activation of small peptides, The Journal of Physical Chemistry A 103 (1999) 3981–3990. doi:10.1021/jp984712b.

[24] D. Ortiz, J.-Y. Salpin, K. Song, R. Spezia, Galactose-6-sulfate collision induced dissociation using qm+mm chemical dynamics simulations and esi-ms/ms experiments, International Journal of Mass Spectrometry 358 (2014) 25–35. doi:10.1016/j.ijms.2013.11.002.

[25] M. D. Hanwell, D. E. Curtis, D. C. Lonie, T. Vandermeersch, E. Zurek, G. R. Hutchison, Avogadro: An advanced semantic chemical editor, visualization, and analysis platform., Journal of cheminformatics 4 (2012) 17. doi:10.1186/1758-2946-4-17.

[26] V. Macaluso, D. Scuderi, M. E. Crestoni, S. Fornarini, D. Corinti, E. Dalloz, E. Martinez-Nunez, W. L. Hase, R. Spezia, L -cysteine modified by s-sulfation: Consequence on fragmentation processes elucidated by tandem mass spectrometry and chemical dynamics simulations, Journal of Physical Chemistry A 123 (2019) 3685–3696. doi:10.1021/acs.jpca.9b01779.

[27] G. L. Barnes, K. Young, L. Yang, W. L. Hase, Fragmentation and reactivity in collisions of protonated diglycine with chemically modified perfluorinated alkylthiolate-self-assembled monolayer surfaces., The Journal of Chemical Physics 134 (2011) 094106. doi:10.1063/1.3558736.

[28] Z. Homayoon, S. Pratihar, E. Dratz, R. Snider, R. Spezia, G. L. Barnes, V. Macaluso, A. M. Somer, W. L. Hase, Model simulations of the thermal dissociation of the tik(h ¡sup¿+¡/sup¿) ¡sub¿2¡/sub¿ tripeptide: Mechanisms and kinetic parameters, The Journal of Physical Chemistry A 120 (2016) 8211–8227. doi:10.1021/acs.jpca.6b05884.

[29] M. Gu, J. Zhang, W. L. Hase, L. Yang, Direct dynamics simulations of the thermal fragmentation of a protonated peptide containing arginine, ACS Omega 5 (2020) 1463–1471. doi:10.1021/acsomega.9b03091.

[30] J. P. Stewart, Mopac2016 (2016).

[31] G. H. Peslherbe, H. Wang, W. L. Hase, Monte carlo sampling for classical trajectory simulations, Advances in Chemical Physics 105 (1999) 171–201. doi:10.1002/9780470141649.

[32] C. Schlier, A. Seiter, High-order symplectic integration: An assess-

ment, Comput. Phys. Commun. 130 (2000) 176–189. doi:10.1016/S0010-4655(00)00011-4.

[33] J. P. Stewart, Mopac2012 (2012).

[34] J. J. P. Stewart, Optimization of parameters for semiempirical methods v: modification of nddo approximations and application to 70 elements., Journal of molecular modeling 13 (2007) 1173–213. doi:10.1007/s00894-007-0233-4.

[35] Z. Gregg, W. Ijaz, S. Jannetti, G. L. Barnes, The role of proton transfer in surface-induced dissociation, The Journal of Physical Chemistry C 118 (2014) 22149–22155. doi:10.1021/jp507069x.

[36] S. A. Vázquez, X. L. Otero, E. Martinez-Nunez, A trajectory-based method to explore reaction mechanisms, Molecules 23 (2018) 3156. doi:10.3390/molecules23123156.

[37] A. Rodríguez, R. Rodríguez-Fernández, S. A. Vázquez, G. L. Barnes, J. J. P. Stewart, E. Martínez-Núñez, tsscds2018: A code for automated discovery of chemical reaction mechanisms and solving the kinetics, Journal of Computational Chemistry 39 (2018) 1922–1930. doi:10.1002/jcc.25370.

[38] M. J. Frisch, G. W. Trucks, H. B. Schlegel, G. E. Scuseria, M. A. Robb, J. R. Cheeseman, G. Scalmani, V. Barone, G. A. Petersson, H. Nakatsuji, X. Li, M. Caricato, A. V. Marenich, J. Bloino, B. G. Janesko, R. Gomperts, B. Mennucci, H. P. Hratchian, J. V. Ortiz, A. F. Izmaylov, J. L. Sonnenberg, D. Williams-Young, F. Ding, F. Lipparini, F. Egidi, J. Goings, B. Peng, A. Petrone, T. Henderson, D. Ranasinghe, V. G. Zakrzewski,

J. Gao, N. Rega, G. Zheng, W. Liang, M. Hada, M. Ehara, K. Toyota, R. Fukuda, J. Hasegawa, M. Ishida, T. Nakajima, Y. Honda, O. Kitao, H. Nakai, T. Vreven, K. Throssell, J. A. M. Jr., J. E. Peralta, F. Ogliaro, M. J. Bearpark, J. J. Heyd, E. N. Brothers, K. N. Kudin, V. N. Staroverov, T. A. Keith, R. Kobayashi, J. Normand, K. Raghavachari, A. P. Rendell, J. C. Burant, S. S. Iyengar, J. Tomasi, M. Cossi, J. M. Millam, M. Klene, C. Adamo, R. Cammi, J. W. Ochterski, R. L. Martin, K. Morokuma, O. Farkas, J. B. Foresman, D. J. Fox, Gaussian 16 revision c.01, gaussian Inc. Wallingford CT (2016).

[39] A. L. Patrick, C. N. Stedwell, B. Schindler, I. Compagnon, G. Berden, J. Oomens, N. C. Polfer, Insights into the fragmentation pathways of gas-phase protonated sulfoserine, International Journal of Mass Spectrometry (12 2014). doi:10.1016/j.ijms.2014.12.001.